Petroleum Science 22 (2025) 4492–4503

Contents lists available at ScienceDirect

Petroleum Science

journal homepage: www.keaipublishing.com/en/journals/petroleum-science

Original Paper

Physic-guided multi-azimuth multi-type seismic attributes fusion for multiscale fault characterization

Lei Song [a,b,c,d], Xing-Yao Yin [b,c,d,*], Ying Shi [a], Kun Lang [b,c,d], Hao Zhou [b,c,d], Wei Xiang [b,c,d]

[a] School of Earth Science, Northeast Petroleum University, Daqing, 163318, Heilongjiang, China
[b] State Key Laboratory of Deep Oil and Gas, China University of Petroleum (East China), Qingdao, 266580, Shandong, China
[c] School of Geosciences, China University of Petroleum (East China), Qingdao, 266580, Shandong, China
[d] Laoshan Laboratory, Qingdao, 266580, Shandong, China

ARTICLE INFO

Article history:
Received 3 January 2025
Received in revised form
3 May 2025
Accepted 30 June 2025
Available online 5 July 2025

Edited by Meng-Jiao Zhou

Keywords:
Fault characterization
Multi-azimuth seismic coherence
Multi-azimuth seismic curvature
Data fusion
Deep learning
Physic-guided neural network

ABSTRACT

Accurate characterization of the fault system is crucial for the exploration and development of fractured reservoirs. The fault characterization technique based on multi-azimuth and multi-attribute fusion is a hotspot. In this way, the fault structures of different scales can be identified and the characterization details of complex fault systems can be enriched by analyzing and fusing the fault-induced responses in multi-azimuth and multi-type seismic attributes. However, the current fusion methods are still in the stage of violent information stacking in utilizing fault information of multi-azimuth and multi-type seismic attributes, and the fault or fracture semantics in multi-type attributes are not fully considered and utilized. In this work, we propose a physic-guided multi-azimuth multi-type seismic attributes intelligent fusion method, which can mine fracture semantics from multi-azimuth seismic data and realize the effective fusion of fault-induced abnormal responses in multi-azimuth seismic coherence and curvature with the cooperation of the deep learning model and physical knowledge. The fused result can be used for multi-azimuth comprehensive characterization for multi-scale faults. The proposed method is successfully applied to an ultra-deep carbonate field survey. The results indicate the proposed method is superior to self-supervised-based, principal-component-analysis-based, and weighted-average-based fusion methods in fault characterization accuracy, and some medium-scale and microscale fault illusions in multi-azimuth seismic coherence and curvature can be removed in the fused result.

1. Introduction

The fault system is the main storage space and migration channel of oil and gas, and it can control oil and gas distribution and determine oil and gas recovery. Accurate characterization of the fault system is crucial for the exploration and development of fractured reservoirs (Chen et al., 2020, 2023; Xiang et al., 2022; Ma et al., 2022). The seismic attribute technology is a reliable means for interpreting reservoir fracture information, especially in ultra-deep exploration surveys with scarce logging data. The seismic coherence is a discontinuity-detection attribute, which can highlight the characteristics of seismic discontinuity caused by sedimentary processes, reservoir boundaries, and tectonic movements (Bahorich and Farmer, 1995; Li et al., 2021a). The discontinuity can be applied to identify and characterize large-scale faults. The higher coherence value indicates the strata are more continuous, and otherwise, it suggests the existence of faults or abnormal geologic bodies. The seismic curvature is a geometric attribute, which indicates the bending degree at a point on the stratum. The rock will break when the formation bends, so the seismic curvature is highly correlated with the development of the fault. The larger curvature value indicates a stronger development of fault. It can be applied to describe the development characteristics of medium-scale or microscale faults (Roberts, 2001; Chopra and Marfurt, 2007; Di and Gao, 2016).

* Corresponding author.
E-mail address: xyyin@upc.edu.cn (X.-Y. Yin).
Peer review under the responsibility of China University of Petroleum (Beijing).

https://doi.org/10.1016/j.petsci.2025.06.022

Limited by the parameters of the observation system, the fault system cannot be fully described by the current post-stacked seismic coherence and seismic curvature due to the narrow observation angle. Rich azimuth information can be mined from wide-azimuth seismic data, which brings great improvement in imaging and fine characterization of complex fault systems (Manning et al., 2007; Barley and Summers, 2007; Chen and Zong, 2022; Chen et al., 2023). The multi-azimuth seismic coherence and multi-azimuth seismic curvature are calculated based on multi-azimuth seismic data (Qi et al., 2017). To mine and utilize azimuthal anisotropy information induced by the fault from seismic data and comprehensively characterize the fault system, the multi-azimuth multi-type seismic attributes fusion method is developed (Li et al., 2015; Shi et al., 2018). The fault information of different attributes and different azimuths can be fused with fusion methods. Faults of different scales can be identified, details of complex faults can be enriched, and imaging accuracy of the fault system can be improved with fused results (Zhou and Zhong, 2024).

The seismic attribute fusion methods can be mainly divided into the transform domain fusion method, spatial domain fusion method, and deep learning fusion method. In the transform domain fusion method, the original seismic attributes are decomposed into sub-datasets using different transform coefficients. Then sub-datasets are fused according to the preset fusion rules, and the fusion attributes are obtained by inverse transformation. Classical transform domain fusion methods include the fusion method based on principal component analysis (PCA) and the fusion method based on the color model (RGB) (Yan et al., 2022; Wang et al., 2023). The calculation error in the process of attribute decomposition, fusion, and reconstruction will be introduced in transform domain fusion methods. Compared with the original seismic attributes, accuracy degradation generally exists in the fused attribute.

In spatial domain methods, the fusion is usually based on some spatial features of the original azimuthal seismic attributes. Compared with the transform domain method, the inverse transformation process of the fused attribute does not need to be reconstructed (Song et al., 2024). Moreover, it focuses on the advantageous observation regions of original multi-azimuth seismic attributes. Higher resolution can be obtained with this method. However, the information in a single pixel or its local neighborhood is considered and used in the fusion process, so some inevitable problems of noise sensitivity and fusion boundary artifacts generally exist in the spatial domain method. In addition, it is worth noting that current spatial domain methods are suitable for the fusion of the single attribute of different azimuths due to the azimuth-focusing assumption.

Recently, the wide applications and excellent performance of deep learning methods in seismic inversion, fault identification, and seismic facies classification have made it widely concerned and applied in the field of seismic attribute fusion (Xiong et al., 2018; Liu et al., 2020; Song et al., 2022; Sun and Zong, 2023; Sun et al., 2024). Deep learning fusion methods can be divided into supervised type and unsupervised type. The deep learning model is trained based on the labeled attribute fusion dataset in the supervised type. The mapping relationship between multi-azimuth seismic attributes and the fused seismic attribute can be learned by deep neural networks, and the high-quality fusion attribute can be generated based on well-trained networks (Cheng et al., 2022). On the other hand, a large amount of unlabeled multi-azimuth and multi-type seismic attributes are used to train the model in the unsupervised method. The problem of label dependence on the fused attribute can be completely overcome in this way. Clustering is the most commonly used approach. The correlation and difference of original seismic attributes are mined to guide the fusion of multi-azimuth and multi-type attributes (Li et al., 2021b). Accordingly, a complex training strategy is necessary to extract common fault features of attributes. Moreover, the physical meaning of the fused result is ambiguous for lacking geologic interpretation and calibration. Consequently, the stability and credibility of the fused results are deficient.

In conclusion, the seismic attribute fusion method is still in its infancy, and the following problems exist in the current fusion methods. 1) The existing fusion methods are mainly based on a single seismic attribute. The fault information contained in the single attribute information is insufficient, so it is difficult to interpret the multi-scale fault information of the reservoir. 2) The abnormal responses of seismic coherence and curvature may be caused by seismic noise or intense geological structural changes (faults, fractures, sediments, rivers, etc.). The current fusion method is still in the stage of violent information stacking in utilizing fault information of multi-type seismic attributes, and the fault or fracture semantics in multi-type attributes are not fully considered and utilized. In other words, the fault features in coherence and the curvature attributes cannot be effectively extracted, and non-fault features cannot be removed in the fusion, which brings abnormal fault illusions in the fused result. 3) The label of deep learning data fusion methods is directly derived from well-logging fault interpretation data, such as coring data, borehole imaging data, and fracture porosity. The amount of labeled data cannot meet the training needs for the high logging cost, which brings the over-fitting problem in the supervised method. On the other hand, the stability and credibility of unsupervised methods are deficient for lacking geologic interpretation and calibration.

In this work, we innovatively propose a physic-guided multi-azimuth multi-type seismic attributes intelligent fusion method, which can realize the effective fusion of multi-azimuth coherence and multi-azimuth curvature using a physic-guided deep learning model. The fused result can be used for fault characterization. Compared with previous approaches, the following innovative works have been done: 1) A novel attribute fusion workflow based on deep learning and physics knowledge is proposed, which avoids the demand for well-logging fracture interpretation data in conventional deep learning fusion methods. 2) The fracture-coupled parameters inversion network (FPI-net) is designed, which can extract the fault or fracture semantics with the assistance of the seismic forward modeling theory of anisotropic media. 3) The multi-azimuth multi-type seismic attributes fusion model is established based on the FPI-net and Bakulin approximation formula (Bakulin et al., 2000), which realizes the effective fusion of fault-induced abnormal responses in multi-azimuth seismic coherence and curvature.

2. Method

2.1. Physic-guided multi-azimuth multi-type seismic attributes fusion workflow

The seismic coherence uses discontinuity to characterize large-scale faults, and the seismic curvature applies stratum bending degree to describe medium-scale or microscale faults. Due to the different observation azimuths, response scales, and physical properties, the description of the fault system by multi-azimuth multi-type seismic attributes is diverse. The attributes fusion method can be applied to integrate fault information from multi-azimuth multi-type seismic attributes, and the fused attribute can be used to characterize the fault system comprehensively and finely.

In previous fusion studies, the deep learning model is applied to establish the direct relationship from multi-azimuth multi-type seismic attributes to the fused attribute. The established relationship can be described as follows:

$$y(t) = f(x_{\mathrm{coh}}(\varphi, t), x_{\mathrm{cur}}(\varphi, t)) \tag{1}$$

$$y(t) = \arg\min\left\{L\left(y(t), y^{\mathrm{L}}(t)\right)\right\} \tag{2}$$

$$L(a, \tilde{a}) = \frac{1}{N}\sum_{i \in C}(a_i - \tilde{a}_i)^2 \tag{3}$$

where x_{coh} and x_{cur} are multi-azimuth seismic coherence and multi-azimuth seismic curvature, which are sequences of azimuth φ and time t. y is the fused attribute, which is the sequence of time t. $f(\cdot)$ is the mapping function, which can be learned by deep learning model based on Eq. (2). y^{L} is the label, $L(\cdot)$ is the function of mean squared error and the definition is given in Eq. (3).

Limited by high drilling costs and data circulation barriers between different surveys, it is not feasible to collect diverse and plentiful label samples to train the model. Consequently, the above fusion formula is not suitable for the field survey with scarce well-logging data, and it needs to be adjusted. Firstly, we assume that the fused attribute can be directly extracted from the multi-azimuth seismic data, that is, the fused attribute is the function of seismic data. In addition, the seismic coherence and curvature of trace i are calculated based on the seismic data of trace i and its neighborhood, so the fused attribute of trace i is the function of the seismic data of trace i and its square neighborhood ($(2k+1)\times(2k+1)$ traces). Finally, we assume that the fused attribute can be used to characterize the degree of fault development. In other words, the fused attribute must preserve fault features of the multi-azimuth coherences and curvatures, and remove the non-fault features. Accordingly, a minimum error exists between the fused attribute and the fault-induced curvature response and coherent response. In this work, an approximate physical formula coupled with fracture parameters and a forward model for HTI medium are introduced to assist the fracture or fault feature extraction of seismic, coherence, and curvature. The adjusted fusion formula is as follows:

$$y(t) = f(x_{\mathrm{sei}}(\varphi, t, i, c)) \tag{4}$$

where x_{sei} is multi-azimuth seismic data, which is the sequence of azimuth φ, time t, inline i, crossline c; $f(\cdot)$ is the mapping function, which can be optimized using Eq. (5); $x^{\mathrm{f}}_{\mathrm{coh}}$ and $x^{\mathrm{f}}_{\mathrm{cur}}$ are azimuth-fused seismic coherence and curvature, which are the sequences of time t; x_{sei0} and $x^{\mathrm{rc}}_{\mathrm{sei0}}$ are input seismic data (center trace) and reconstructed seismic data (center trace) using physics model, which are sequences of azimuth φ, time t; α, β, γ are artificial confidence parameters.

Here, we establish a physic-guided multi-azimuth multi-type seismic attributes fusion workflow to learn the mapping function described in Eq. (4). The established workflow is given in Fig. 1. It mainly consists of the following four modules: the fracture-coupled parameters inversion network (FPI-net, detailed in Section 2.2), the Bakulin approximation formula (detailed in Section 2.2), the forward model for horizontally transverse isotropic (HTI) medium (detailed in Section 2.3), and the multi-azimuth attributes fusion model (detailed in Section 2.4).

The FPI-net is designed to predict fracture-coupled parameters from seismic data. The input is the standardized 4D seismic spatio-temporal sequence with dimension of $(N_\varphi, N_t, N_i, N_c)$. The output is fracture-coupled parameters with dimension of $(5,\ N_t,\ 1,\ 1)$, including background P-wave module, background S-wave module, background density, normal weakness, and tangential weakness. The N_φ, N_t, N_i, and N_c represent the number of azimuth, time samples, inline, and crossline. The fracture-coupled parameters can be converted to the fracture indicator $(1, N_t, 1, 1)$ with the Bakulin approximation formula. The FPI-net and Bakulin approximation formula form the multi-azimuth multi-type seismic attributes fusion model. It can be optimized with supervised learning using Eq. (5). The label includes normalized azimuth-fused coherence $(1, N_t, 1, 1)$, normalized azimuth-fused curvature $(1, N_t, 1, 1)$, and standardized input seismic data $(N_\varphi, N_t, 1, 1)$. The purpose of the forward model is to assist the FPI-net in mining fault-related or fracture-related semantics in azimuth-fused coherence, azimuth-fused curvature, and multi-azimuth seismic. The extracted fault-related or fracture-related semantic can be used to guide the fusion of the multi-azimuth multi-type seismic attributes.

The specific data fusion process can be divided into the following stages:

(1) Data processing stage

The task of the data processing stage is to extract multi-azimuth seismic wavelets, establish 4D seismic spatio-temporal sequences, calculate multi-azimuth seismic coherence and curvature, standardize the data, and form a standardized training dataset. Firstly, calibrate the well and seismic to establish the time-depth relationship, and calculate multi-azimuth seismic wavelets based on calibrated well and multi-azimuth seismic data. Secondly, the 4D seismic spatio-temporal sequences $(N_\varphi, N_t, N_i, N_c)$ are established by extracting multi-azimuth seismic data in the 3D rectangular bin with a radius of k trace by trace ($N_i = 2k+1$; $N_c = 2k+1$). Third, multi-azimuth seismic coherence is calculated using the eigen-structure-based coherence method from multi-azimuth seismic data (Gersztenkorn and Marfurt, 1999), multi-azimuth seismic curvature is calculated based on the 3D volumetric multispectral estimation method (Al-Dossary and Marfurt, 2006), and the azimuth-fused coherence and curvature are obtained based on multi-azimuth attributes fusion model (Song et al., 2024). Finally, normalize the azimuth-fused

$$y(t) = \arg\min\left\{\underbrace{\alpha L\left(y(t), 1 - x^{\mathrm{f}}_{\mathrm{coh}}(t)\right)}_{L_{\mathrm{coh}}} + \underbrace{\beta L\left(y(t), x^{\mathrm{f}}_{\mathrm{cur}}(t)\right)}_{L_{\mathrm{cur}}} + \underbrace{\gamma \frac{1}{N_\varphi}\sum_{k=1}^{N_\varphi} L\left(x^{\mathrm{rc}}_{\mathrm{sei0}}(\varphi_k, t, i_0, c_0), x_{\mathrm{sei0}}(\varphi_k, t, i_0, c_0)\right)}_{L_{\mathrm{sei}}}\right\} \tag{5}$$

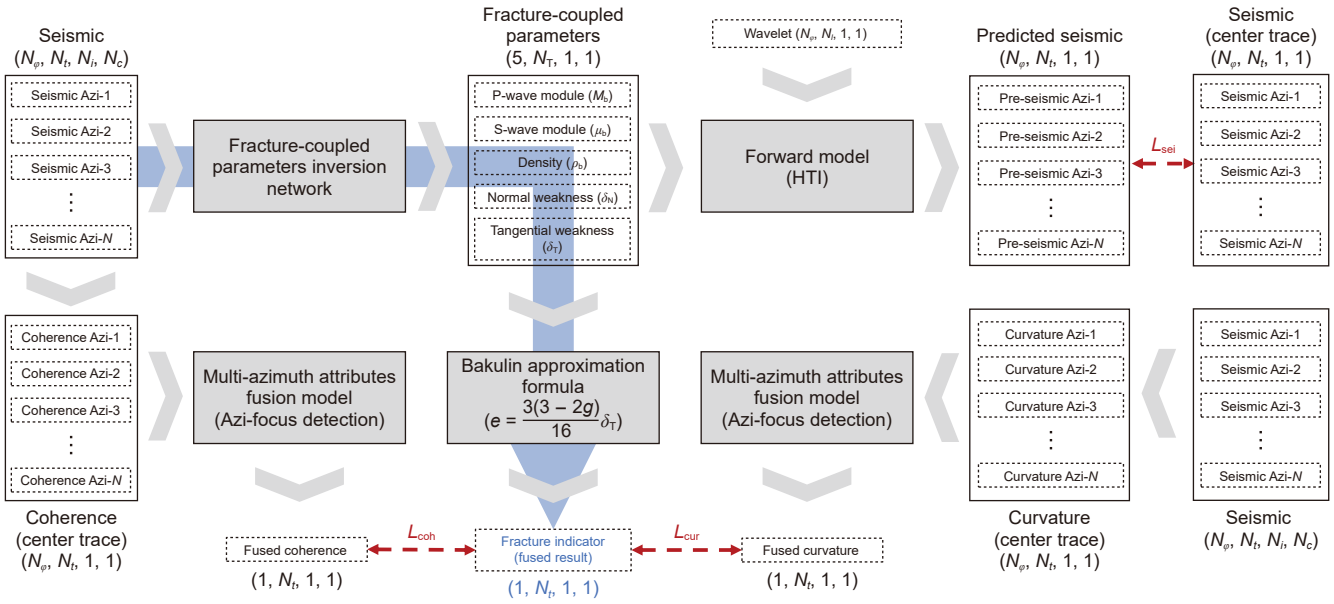

Fig. 1. The physic-guided multi-azimuth multi-type seismic attributes fusion workflow. It mainly consists of the following four modules: the fracture-coupled parameters inversion network, Bakulin approximation formula, forward model for horizontal transverse isotropy (HTI) medium, and multi-azimuth attributes fusion model.

coherence, azimuth-fused curvature, and multi-azimuth seismic wavelet. Standardize the 4D seismic spatio-temporal sequences.

(2) Training stage

The task of the training stage is to adjust learnable parameters in FPI-net based on the standardized training dataset. The objective function given in Eq. (5) is adopted to guide the iterative optimization of FPI-net. It consists of L_{coh}, L_{cur}, and L_{sei} terms. The term L_{coh} is calculated based on the predicted fracture indicator and azimuth-fused coherence, the term L_{cur} is calculated based on the predicted fracture indicator and azimuth-fused curvature, and term L_{sei} is calculated based on predicted seismic data and input 4D seismic spatio-temporal sequence (center trace). The predicted seismic data is obtained using the forward model from fracture-coupled parameters and multi-azimuth seismic wavelets.

(3) Data fusion stage

In this stage, the final fused result (fracture indicator) can be obtained from 4D seismic spatio-temporal sequences using the well-trained FPI-net and Bakulin approximation formula.

2.2. Multi-azimuth multi-type seismic attributes fusion model

The multi-azimuth multi-type seismic attributes fusion model is composed of the FPI-net and Bakulin approximation formula. The FPI-net is designed to predict fracture-coupled parameters from multi-azimuth seismic data, and the Bakulin approximation formula is adopted to convert fracture-coupled parameters to the fracture indicator. The degree of fracture or fault development can be characterized by the fracture indicator.

The convolutional neural network (CNN) is a classical feedforward neural network, which is inspired by animal visual cortex tissue. The complexity of the network can be simplified and the number of learnable parameters of the network can be reduced for local connections and weight sharing. The properties of the underlying strata are related to the properties of the overlying strata. The seismic data is the comprehensive response of the underground medium. The depth of seismic data is time depth. Consequently, it can be considered as the time sequence. When the CNN is used to process time sequences, the interest features within a certain length range can be extracted effectively using sliding convolution operation with a fixed length of convolution kernel. The short-term high-frequency spatio-temporal features in 3D seismic data can be captured with 3D convolution and a fully connected network. The forward propagation process is given in Eq. (6).

$$y_{N_B\times C_{out}\times D_{out}} = \sum_{i=0}^{C_{out}-1}\sum_{j=0}^{C_{in}-1} x(j)_{N_B\times D_{in}} * w(i,j)_{N_B\times D_w} + b_{N_B\times C_{out}\times D_{out}} \tag{6}$$

where x, y, w, and b are input, output, weight kernel, and bias matrix; * is the convolution operation; C_{in}, C_{out} are number of input channels and output channels; N_B is the batch size; D_{in},D_{out}, and D_w represent dimensions of input, output, and kernel.

However, long-term low-frequency features cannot be effectively extracted with CNN. Different from CNN, hidden state variables and recursive structures are adopted in the recurrent neural network (RNN) to capture dependencies in time sequences. The memory ability is realized in this way. The gate recurrent unit (GRU) is a classical RNN, which can be used to solve the problems of long-term memory and gradient disappearance in classical RNN. The forward propagation process is given in Eq. (7). The long-term low-frequency spatio-temporal features in 3D seismic data can be captured with parallel GRUs and a fully connected network.

$$\begin{cases} r_t = \mathrm{Sigmoid}(W_{xr}x_t + W_{hr}h_{t-1} + b_r) \\ u_t = \mathrm{Sigmoid}(W_{xu}x_t + W_{hu}h_{t-1} + b_u) \\ \tilde{h}_t = \mathrm{Tanh}(W_{xh}x_t + W_{hh}(r_t \odot h_{t-1}) + b_h) \\ h_t = u_t h_{t-1} + (1-u_t)\odot \tilde{h}_t \\ y_t = \mathrm{Tanh}\left(W_{hy}h_t + b_y\right) \end{cases} \tag{7}$$

where x_t and y_t are the input and output at time t; r_t and u_t are reset gate signal and update gate signal; h_{t-1} and h_t are state variables at time t and $t-1$, which are used to store the information at time $t-1$ and $t-2$, W and b are weight matrices and bias matrices; and the operator $\odot$ represents Hadamard product.

The purpose of the fully connected network is to connect the extracted features. In this work, it is used to fuse the features from 3D convolution units to obtain short-term high-frequency spatio-temporal features and fuse the features from GRUs to obtain long-term low-frequency spatio-temporal features. In addition, it can be applied to establish the mapping relationship between different domains. The forward propagation process is presented in Eq. (8).

$$y_{N_B\times C_{out}\times D_{out}} = \sum_{i=0}^{C_{out}-1}\sum_{j=0}^{C_{in}-1} x(j)_{N_B\times D_{in}} \times w(i,j)_{N_B\times D_w} + b_{N_B\times C_{out}\times D_{out}} \tag{8}$$

where x, y, w, and b are input, output, weight matrix, and bias matrix.

The batch normalization layer and the activation function are generally used in conjunction with the above network units. The batch normalization layer is used to solve internal covariate shifts and accelerate the training speed, and the activation function is to supply the nonlinear factor. The definitions are as follows:

$$y_{N_B\times D} = \lambda\frac{x_{N_B\times D} - \mu_B}{\sqrt{\sigma_B^2 + \varepsilon}} + \gamma \tag{9}$$

$$\mathrm{Sigmoid}(x) = \frac{1}{1+e^{-x}} \tag{10}$$

where μ_B and σ_B^2 are mean and variance of the batch data, λ and γ are learnable parameters, ε is a very small value added to the denominator for numerical stability.

Finally, the FPI-net is established based on 3D convolution units, GRUs, fully connected units, batch normalization layers, and Sigmoid activation functions. The structure is displayed in Fig. 2.

The FPI-net includes the long-term low-frequency spatio-temporal pattern analysis module, the short-term high-frequency spatio-temporal pattern analysis module, and the regression module. In the long-term low-frequency spatio-temporal pattern analysis module, the input seismic is split into $N_i \times N_c$ seismic sub-sequences, and parallel stacked three-layer GRUs are adopted to mine long-term low-frequency temporal features from seismic sub-sequences. The long-term low-frequency spatio-temporal features can be obtained by concatenating feature sub-sequences. The extracted feature information of the third and fourth dimensions is fused using a fully connected layer. On the other hand, the short-term low-frequency spatio-temporal features can be obtained in the short-term high-frequency spatio-temporal pattern analysis module. Firstly, three parallel 3D convolution structures with multi-scale reception fields are applied to extract multi-scale short-term spatio-temporal features, which are realized by setting the same kernel size and multi-scale padding and dilation parameters in 3D convolution layers. The 3D convolution structure is composed of a 3D convolution layer, a batch normalization layer, and a Sigmoid activation function. Then multi-scale features are fused by serial three-layer 3D

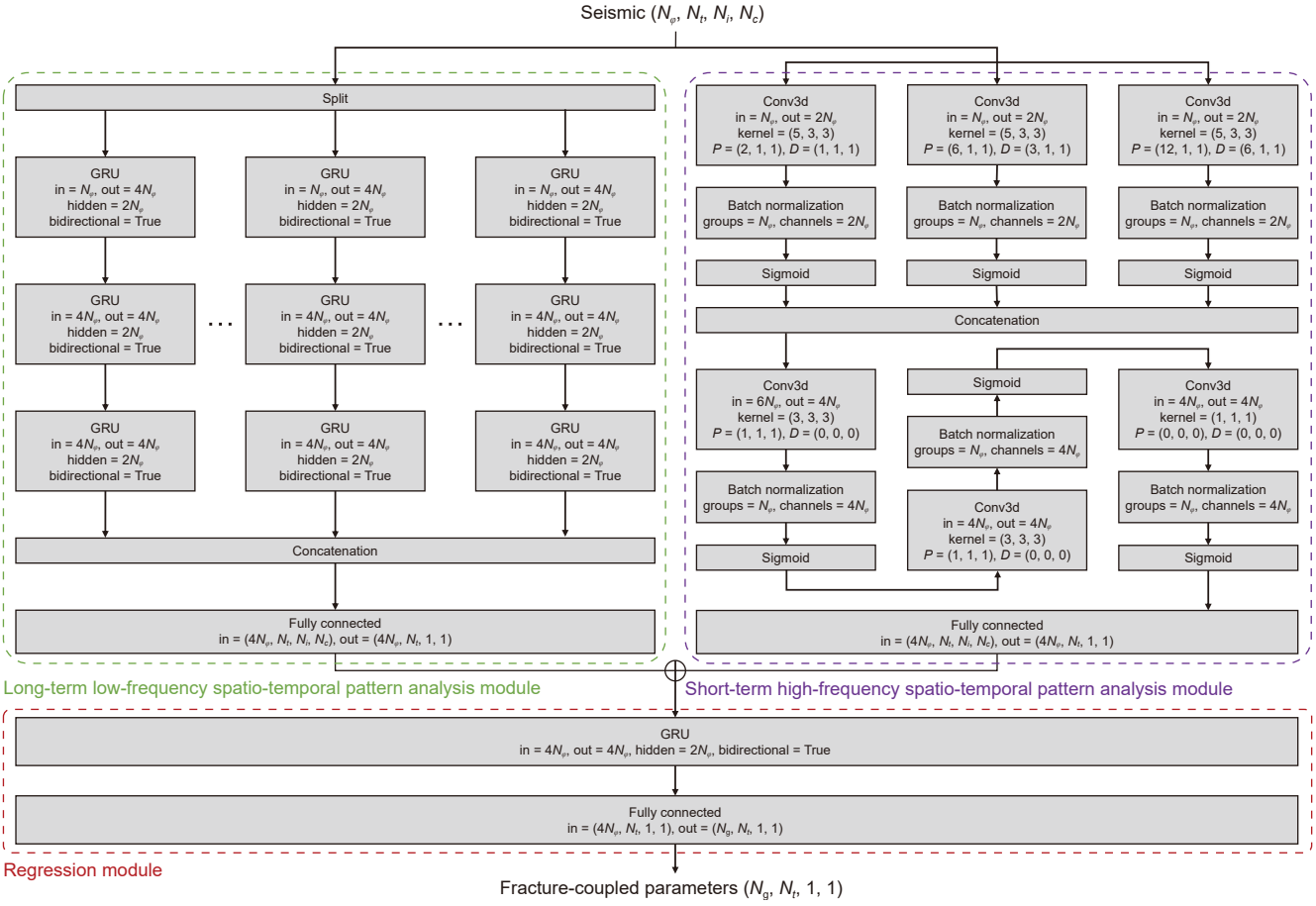

Fig. 2. The structure of fracture-coupled parameters inversion network (FPI-net). It is established based on 3D convolution units, GRUs, fully connected units, batch normalization layers, and Sigmoid activation functions.

convolution structures. Finally, a fully connected layer is adopted to fuse the extracted feature information of the third and fourth dimensions. The function of the final regression module is to establish the mapping relation from the feature domain to the target domain. It includes a GRU and a fully connected layer. The input is the summation of the output of the above two modules, and the output is fracture-coupled parameters.

Bakulin et al. (2000) derived the relationship between the tangential weakness and fracture density in fluid-filled fractures. The definition is given in Eq. (11):

$$e = \frac{3(3-2g)}{16}\delta_{\mathrm{T}} \tag{11}$$

where e is fracture density, δ_{T} represent tangential weakness, and parameter g is defined as

$$g = \frac{{V_{\mathrm{S}}}^2}{{V_{\mathrm{P}}}^2} \tag{12}$$

where V_{S} and V_{P} are the S-velocity and P-velocity in the background medium.

2.3. Forward model for horizontally transverse isotropic medium

In our work, the approximate reflection coefficient equation for the horizontally transverse isotropic medium and the seismic convolution model are designed as the forward model due to massive vertical fractures developed in the target reservoir. The azimuthal reflection coefficient can be calculated from fracture-coupled parameters using the approximate reflection coefficient equation. The definition is presented in Eqs. (13)–(15) (Pan et al., 2018, 2019).

$$R_{\mathrm{HTI}}(\theta,\varphi) = a_M(\theta)\frac{\Delta M_{\mathrm{b}}}{M_{\mathrm{b}}} + a_\mu(\theta)\frac{\Delta\mu_{\mathrm{b}}}{\mu_{\mathrm{b}}} + a_\rho(\theta)\frac{\Delta\rho_{\mathrm{b}}}{\rho_{\mathrm{b}}} + a_{\delta_{\mathrm{N}}}(\theta,\varphi)\Delta\delta_{\mathrm{N}} + a_{\delta_{\mathrm{T}}}(\theta,\varphi)\Delta\delta_{\mathrm{T}} \tag{13}$$

$$\begin{cases} a_M(\theta) = \dfrac{\sec^2\theta}{4}, a_\mu(\theta) = -(1-\chi_{\mathrm{b}})\sin^2\theta, a_\rho(\theta) = \dfrac{1}{2} - \dfrac{\sec^2\theta}{4}, \\ a_{\delta_{\mathrm{N}}}(\theta,\varphi) = -\dfrac{\sec^2\theta}{4}\left[1-(1-\chi_{\mathrm{b}})\left(\sin^2\theta\sin^2\varphi + \cos^2\theta\right)\right]^2, \\ a_{\delta_{\mathrm{T}}}(\theta,\varphi) = \dfrac{1-\chi_{\mathrm{b}}}{2}\sin^2\theta\cos^2\varphi\left(1-\tan^2\theta\sin^2\varphi\right) \end{cases} \tag{14}$$

$$\chi_{\mathrm{b}} = \lambda_{\mathrm{b}}/M_{\mathrm{b}} = 1 - 2\mu_{\mathrm{b}}/M_{\mathrm{b}} \tag{15}$$

where M_{b} is background P-wave module, μ_{b} is background S-wave module, ρ_{b} is background density, δ_{N} is normal weakness, δ_{T} is tangential weakness, θ incidence angle, φ is azimuth angle, λ_{b} and μ_{b} are background Lame parameter.

Based on the calculated azimuthal reflection coefficient and seismic wavelet, we can generate the azimuthal seismic data with the seismic convolution model. Its definition is given in Eq. (16).

$$S(\theta,\varphi) = R_{\mathrm{HTI}}(\theta,\varphi) * w(\theta,\varphi) \tag{16}$$

where S is azimuthal seismic data, w is seismic wavelet, and the operator * represents convolution operation.

2.4. Multi-azimuth attributes fusion model

The seismic discontinuity can be highlighted with seismic coherence, enabling it to identify large-scale faults. The seismic curvature can be applied to describe the development characteristics of medium-scale faults by calculating the bending degree of the stratum. In this work, the multi-azimuth seismic coherence and curvature are calculated based on the eigen-structure-based seismic coherence algorithm and 3D volumetric multispectral estimation seismic curvature algorithm (Gersztenkorn and Marfurt, 1999; Al-Dossary and Marfurt, 2006). The multi-azimuth attributes fusion model is based on azimuth focus detection, which can effectively fuse the multi-azimuth information of a single attribute to reflect the characteristics of geological bodies comprehensively and credibly (Song et al., 2024). It is applied to fuse multi-azimuth information of multi-azimuth seismic coherence and curvature respectively. The specific implementation process is as follows:

1) The guided filter is adopted to enhance the edge characteristics of faults on the multi-azimuth seismic attribute. Here the input multi-azimuth seismic attribute is adopted as the guided attribute. The output of the guided filter is given in Eq. (17).

$${x_\varphi}^{\mathrm{g}} = f_{\mathrm{g}}(x_\varphi, x_\varphi) \tag{17}$$

where x_φ is multi-azimuth seismic attribute (coherence or curvature), ${x_\varphi}^{\mathrm{g}}$ represents the output of the guided filter, and f_{g} is the guided filter.

2) Meanwhile, the average filtering is performed on the multi-azimuth seismic attribute to extract background characteristics. The output of the average filter is given in Eq. (18).

$${x_\varphi}^{\mathrm{a}} = f_{\mathrm{a}}(x_\varphi) \tag{18}$$

where ${x_\varphi}^{\mathrm{a}}$ represents the output of the average filter, and f_{a} is the average filter.

3) The absolute difference between the output of the guided filter and the average filter is calculated to obtain the edge information of faults at different azimuths (Eq. (19)), and the guided filtering is performed on the difference to further enhance the edge information of faults (Eq. (20)).

$$d_\varphi = \left|{x_\varphi}^{\mathrm{g}} - {x_\varphi}^{\mathrm{a}}\right| \tag{19}$$

$${d_\varphi}^{\mathrm{g}} = f_{\mathrm{g}}(d_\varphi, d_\varphi) \tag{20}$$

where d_φ is absolute multi-azimuth difference, and ${d_\varphi}^{\mathrm{g}}$ is enhanced absolute multi-azimuth difference.

4) The local standard deviation of enhanced absolute multi-azimuth difference is calculated azimuth by azimuth and point by point. The local standard deviation $\sigma_{\mathrm{D}}(i,j)$ of point (i,j) at the neighborhood $N(i,j)$ is defined in Eq. (21).

$${\sigma_{d_\varphi}}^{\mathrm{g}}{}^2(i,j) = \frac{1}{|N(i,j)|}\sum_{(m,n)\in N(i,j)}\left({d_\varphi}^{\mathrm{g}}(m,n) - \overline{{d_\varphi}^{\mathrm{g}}}(i,j)\right)^2 \tag{21}$$

where $|N(i,j)|$ is the points number of the neighborhood, and $\overline{{d_\varphi}^{\mathrm{g}}}(i,j)$ is the local average of the neighborhood $N(i,j)$.

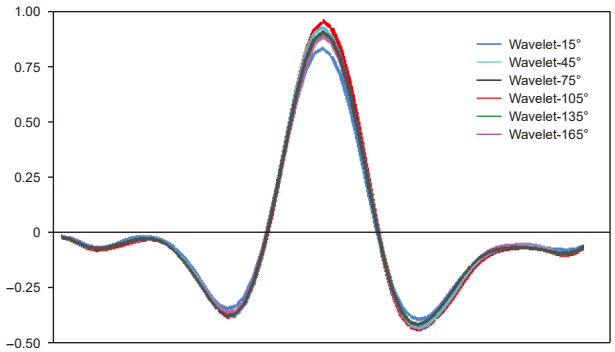

Fig. 3. The normalized seismic wavelets with azimuths of 15°, 45°, 75°, 105°, 135°, and 165°.

5) The edge of faults at advantageous observation azimuth is more obvious than other azimuths. Accordingly, the local standard deviation of enhanced absolute difference at advantageous observation azimuth shows a higher value. The fusion decision map of azimuth φ_k ($\varphi_k \in \varphi$) is established by searching the max local standard deviation, which is given in Eq. (22).

$$M_{\varphi_k}(i,j) = \begin{cases} 1, & \sigma_D(i,j)_{\varphi_k} = \max(\sigma_D(i,j)_{\varphi}) \\ 0, & \sigma_D(i,j)_{\varphi_k} < \max(\sigma_D(i,j)_{\varphi}) \end{cases} \tag{22}$$

where M_{φ_k} is the decision map matrix of azimuth φ_k.

Finally, the multi-azimuth seismic attribute can be fused based on the following formula:

$$x_{\text{fused}} = \sum_{\varphi_k \in \varphi} M_{\varphi_k} \odot x_{\varphi_k} \tag{23}$$

where x_{fused} is the azimuth-fused seismic attribute, and the x_{φ_k} is the seismic attribute of azimuth φ_k.

3. Example

The proposed method is applied to a field survey in northwest China. The target horizon is a typical fracture-cave carbonate reservoir, which is located about 7500–7800 m underground. The multi-type and multi-scale faults and caves are developed in the target horizon. The seismic data is collected using the small acquisition binning and wide azimuth, and it is divided into six azimuthal partial-stacked seismic data with azimuths of 15°, 45°, 75°, 105°, 135°, 165°. Only one inclined well is deployed in the survey due to ultradeep exploration targets. In addition, the well-logging interpretation is incomplete, the imaging logging information is missing, and only several points about reservoir-type interpretation (reservoir, non-reservoir) are available.

The multi-azimuth seismic wavelets are extracted based on calibrated well-logging data and seismic data. The multi-azimuth seismic coherence is calculated using the eigen-structure-based seismic coherence algorithm from multi-azimuth seismic data, and multi-azimuth seismic curvature is calculated based on the maximum positive curvature algorithm. The azimuth-fused seismic coherence and curvature are obtained using the multi-azimuth attributes fusion model based on azimuth focus detection.

In order to reduce the numerical difference of coherence, curvature, and seismic penalty terms in the loss function and improve training efficiency and stability, the multi-azimuth seismic data is standardized with Eq. (24), the azimuth-fused coherence and curvature are normalized with Eq. (25), and the multi-azimuth seismic wavelets are normalized with Eq. (26).

$$Y = \frac{X - \mu}{\sigma} \tag{24}$$

$$Y = \frac{X - X_{\min}}{X_{\max} - X_{\min}} \tag{25}$$

$$Y = \frac{X}{X_{\max}} \tag{26}$$

The multi-azimuth seismic wavelets are presented in Fig. 3. The multi-azimuth seismic amplitude slices, multi-azimuth seismic coherence slices, and multi-azimuth seismic curvature slices along with the target horizon are displayed in Figs. 4–6. The slices of azimuth-fused coherence and azimuth-fused curvature are given in Fig. 7(a) and (b).

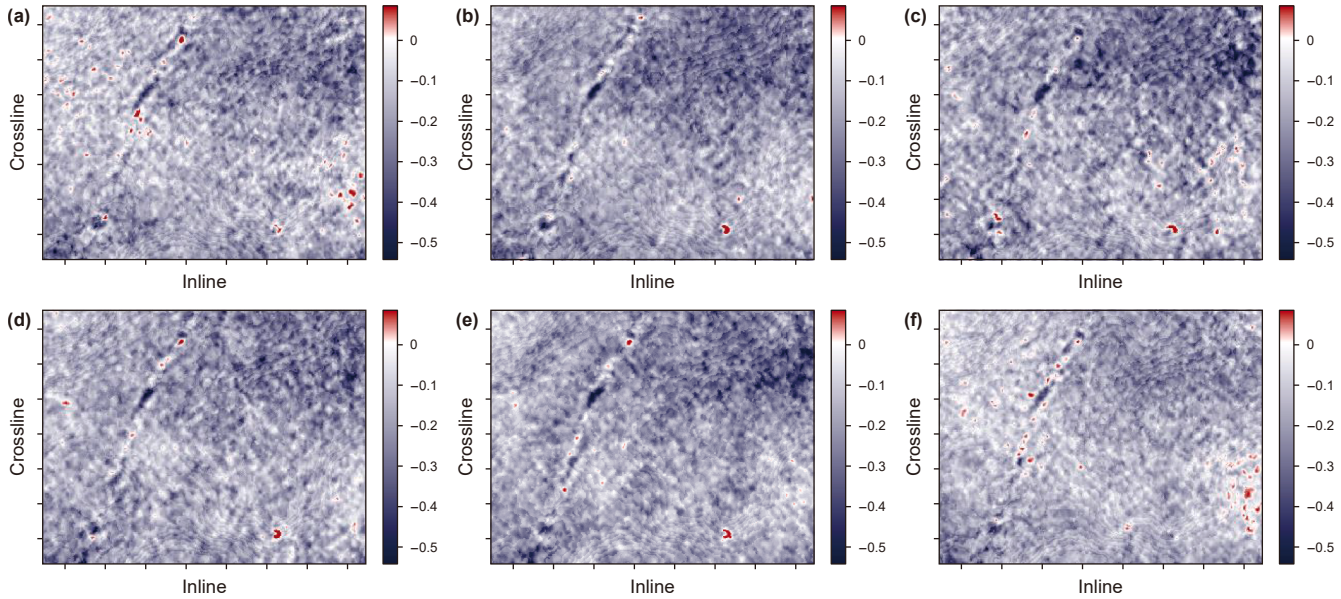

Fig. 4. The seismic amplitude slices along with the target reservoir horizon with azimuths of **(a)** 15°, **(b)** 45°, **(c)** 75°, **(d)** 105°, **(e)** 135°, and **(f)** 165°.

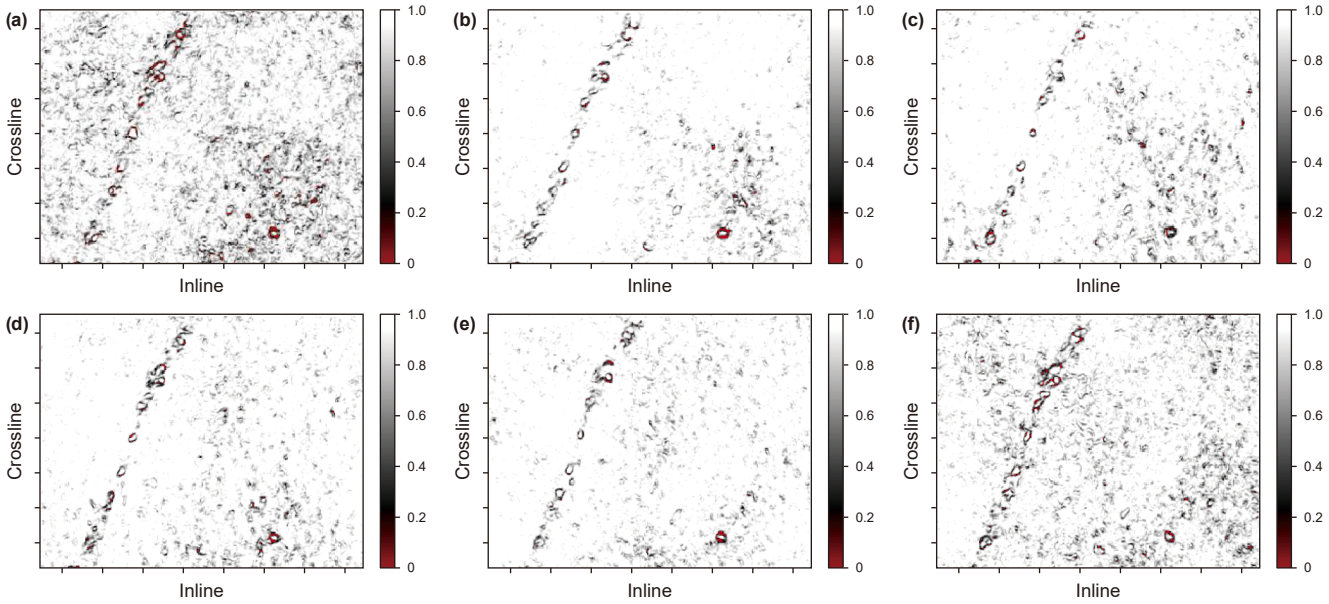

Fig. 5. The seismic coherence slices along with the target reservoir horizon with azimuths of **(a)** 15°, **(b)** 45°, **(c)** 75°, **(d)** 105°, **(e)** 135°, and **(f)** 165°.

Finally, the standard multi-azimuth seismic data, normalized multi-azimuth seismic wavelets, and normalized azimuth-fused seismic coherence and curvature are adopted as training data, and the adaptive moment estimation (Adam) optimizer is applied to adjust learnable parameters in FPI-net. The hyper training parameters are set as follows: the artificial confidence parameters α, β, and γ are 1, 1, and 0.2, the learning rate is 0.005, and the training epoch is 1000. The evolution of training errors is given in Fig. 8. The convergence of the error curves indicates that the model is gradually learning the inherent law of the data and achieving a better fusion effect. The fused result is presented in Fig. 7(f), and we also display the fused results of the weight-average-based fusion method, PCA-based fusion method, and self-supervised-based fusion method in Fig. 7(c)–(e). Compared with the single attribute of a single azimuth, the information contained in fused results is more abundant and the description of the fault system is more comprehensive and detailed. The results in Fig. 7 indicate that the multi-scale fault information from coherence and curvature can be reserved with the above four methods. It is worth noting that the energy of the main fault zone with the proposed method is more prominent and the boundary is clearer with the proposed method. Furthermore, some possible medium-scale and small-scale fault illusions are removed by extracting and utilizing fracture semantics with the proposed method.

To further evaluate the proposed method, we give 2D results through the well (red survey line displayed in Fig. 7). The 2D multi-azimuth seismic data, seismic coherence, and seismic curvature are presented in Figs. 9–11. Fig. 12 shows 2D profiles of azimuth-

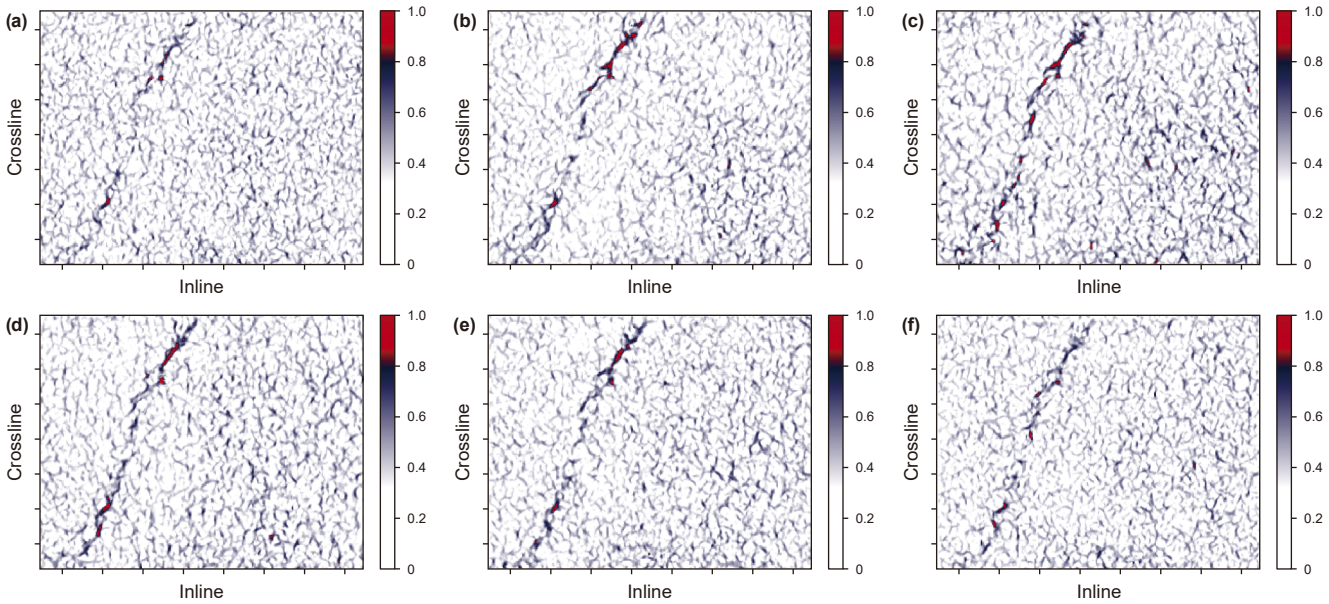

Fig. 6. The seismic curvature slices along with the target reservoir horizon with azimuths of **(a)** 15°, **(b)** 45°, **(c)** 75°, **(d)** 105°, **(e)** 135°, **and (f)** 165°.

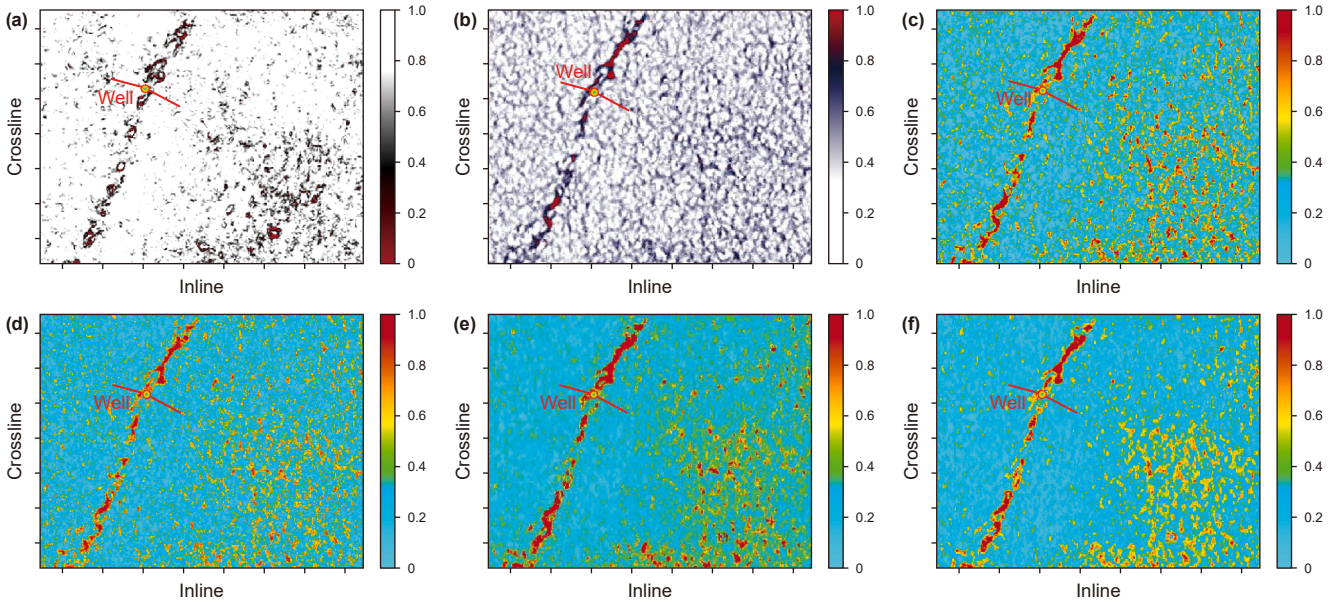

Fig. 7. **(a)**–**(f)** are slices of azimuth-fused seismic coherence, azimuth-fused seismic curvature, and fused results with the weight-average-based fusion method, the PCA-based fusion method, self-supervised-based fusion method, and the proposed method.

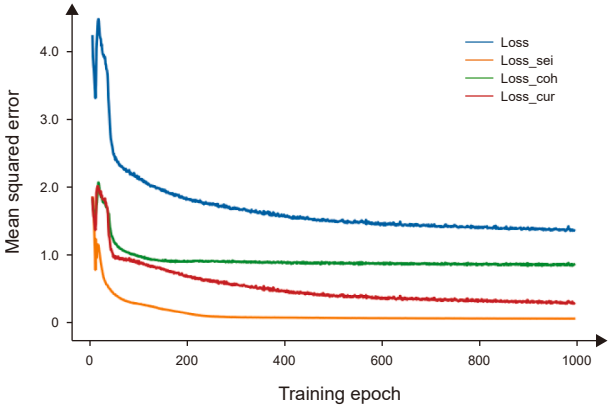

Fig. 8. The evolution of training errors with training epochs.

fused seismic coherence, azimuth-fused seismic curvature, and fused results with the weight-average-based fusion method, the PCA-based fusion method, self-supervised-based fusion method, and the proposed method. By comparing the enlarged fused results and well-logging interpretation of reservoir type in Fig. 12 (c1)–(e1), it can be observed that the consistency between our result and well-logging fracture-cavity interpretation is higher, especially in regions marked by red and black arrows. Furthermore, we can find that the fault illusions (marked by black arrows) in the fused results of weight-average-based, PCA-based, and self-supervised-based fusion methods are caused by strong responses of azimuth-fused coherence, and the fault illusions (marked by red arrows) in the fused result of the weight-average-based fusion method and PCA-based fusion method are caused by the weak responses of azimuth-fused curvature. The abnormal response in the coherence and curvature attributes may be caused by faults, fractures, or other factors (noise, sediments, rivers, etc.). Because the above three methods cannot identify and extract abnormal responses caused by the fractures or faults in the fusion, fracture or fault illusions in the fusion results are inevitable. In contrast, fracture semantics can be extracted with physical knowledge and the deep learning model and it can be applied to guide the fusion in the proposed method, so the fused result can retain fracture-induced abnormal responses and remove non-fracture-induced abnormal responses in seismic attributes.

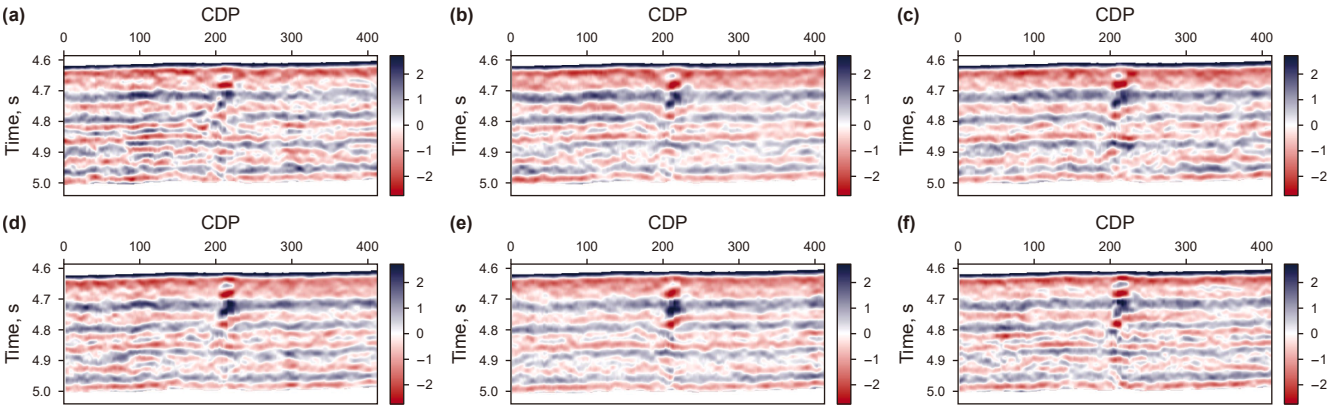

Fig. 9. The seismic profiles with azimuths of **(a)** 15°, **(b)** 45°, **(c)** 75°, **(d)** 105°, **(e)** 135°, and **(f)** 165°.

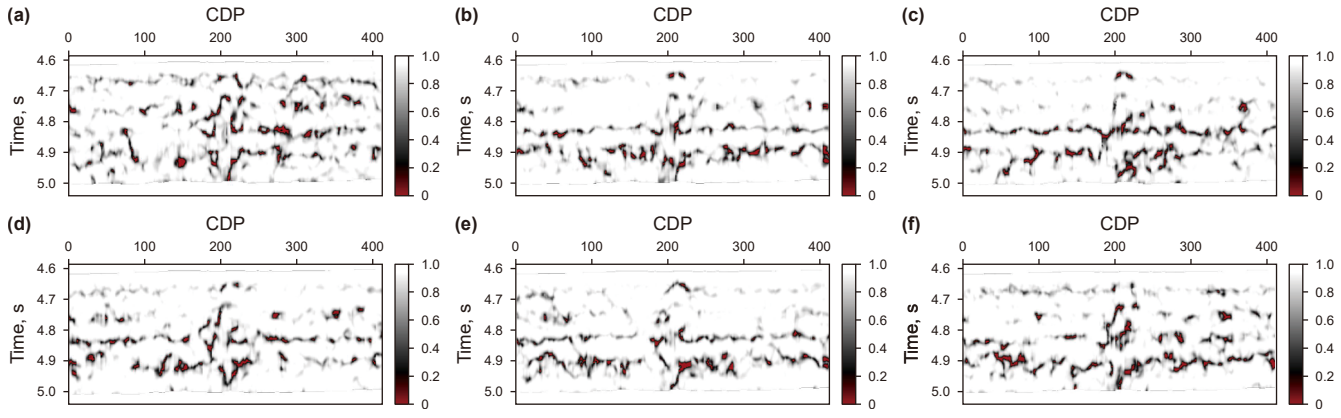

Fig. 10. The seismic coherence profiles with azimuths of **(a)** 15°, **(b)** 45°, **(c)** 75°, **(d)** 105°, **(e)** 135°, **and (f)** 165°.

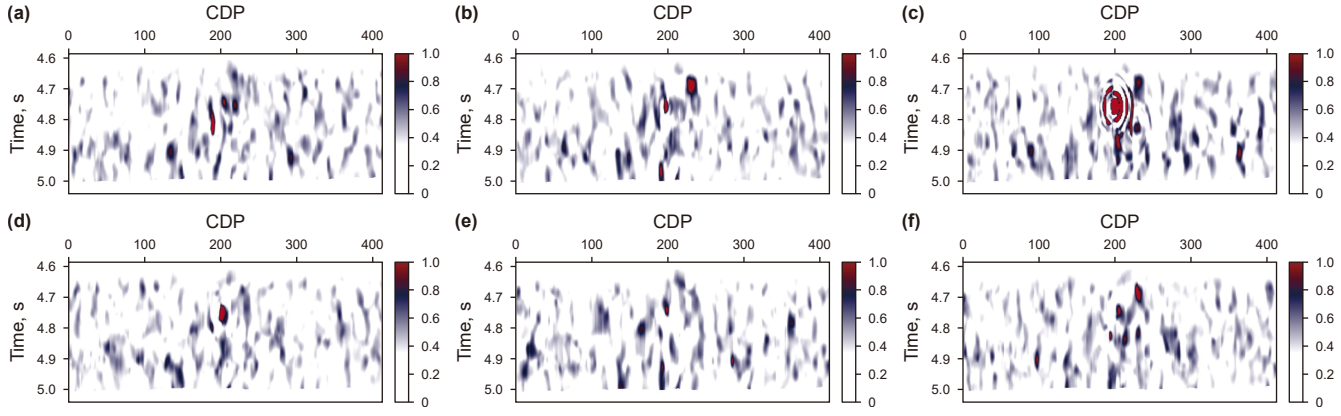

Fig. 11. The seismic curvature profiles with azimuths of **(a)** 15°, **(b)** 45°, **(c)** 75°, **(d)** 105°, **(e)** 135°, and **(f)** 165°.

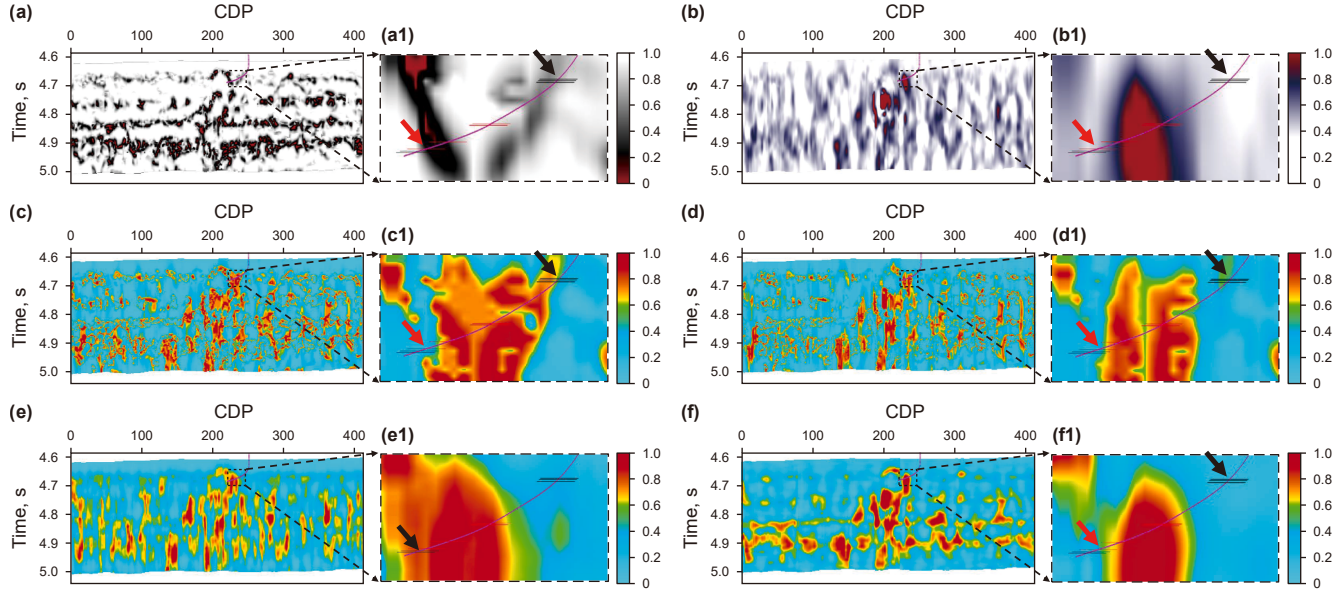

Fig. 12. **(a)**–**(f)** are profiles of azimuth-fused seismic coherence, azimuth-fused seismic curvature, and fused results with the weight-average-based fusion method, the PCA-based fusion method, self-supervised-based fusion method, and the proposed method; **(a1)**–**(f1)** are corresponding enlarged results marked by the black rectangular dotted line in **(a)**–**(f)**; The red lines in the well curve represent the fracture-cavity reservoir, and black lines represent the non-reservoir.

4. Conclusion and discussion

In this work, we propose a physic-guided multi-azimuth multi-type seismic attributes intelligent fusion method, which can realize the effective fusion of fault-induced abnormal responses in multi-azimuth seismic coherence and curvature. The fused result can be used for multi-azimuth comprehensive characterization for multi-scale faults. Specifically, the FPI-net and physical forward models are designed to extract fracture-coupled parameters from multi-azimuth seismic data. The fracture semantic is further mined from fracture-coupled parameters based on the FPI-net and the Bakulin approximation formula. Finally, the mined fracture semantic is used to guide the fusion of multi-azimuth seismic coherence and curvature. In this way, the large-scale and medium-scale fault-induced abnormal responses in multi-azimuth seismic coherence and curvature can be retained in the fused result, non-fault-induced responses in multi-azimuth seismic coherence and curvature can be removed from the fused result, and small-scale fault features in multi-azimuth seismic data can be supplemented to the fused result. The proposed method is successfully applied to an ultra-deep carbonate field survey for multi-scale fault characterization. The results indicate the proposed method is superior to the self-supervised-based, PCA-based, and weighted-average-based fusion methods in fault characterization accuracy, and some medium-scale and small-scale fault illusions in multi-azimuth seismic coherence and curvature can be removed in the fused result. It is worth noting that the proposed method is applicable to target surveys with massive high-dip (approximately 90°) faults/fractures. In practical applications, most faults/fractures in fault-controlled hydrocarbon reservoirs are high-dip ones controlled by multiple sets of in-situ stress fields, with complex intersecting relationships. The complexity of the fracture system may far exceed the descriptive scope of the HTI model. The model considering the intersecting distribution of multiple sets of vertical fractures can more accurately describe the complex fracture system. Consequently, combining the proposed method with the orthogonality anisotropic media (OA) model will be the focus of our future research.

CRediT authorship contribution statement

Lei Song: Resources, Investigation, Conceptualization, Writing – original draft, Methodology, Data curation, Writing – review & editing, Project administration, Formal analysis. **Xing-Yao Yin:** Funding acquisition, Methodology, Supervision. **Ying Shi:** Visualization, Data curation, Formal analysis, Software. **Kun Lang:** Validation, Visualization. **Hao Zhou:** Writing – review & editing. **Wei Xiang:** Data curation, Software.

Declaration of competing interest

The authors declare that they have no known competing financial interests or personal relationships that could have appeared to influence the work reported in this paper.

Acknowledgments

We would like to acknowledge the sponsorship of the National Natural Science Foundation of China (42430809, 42030103) and the Basic Research Funds for Northeast Petroleum University in Heilongjiang Province (2025GPL-01).

References

Al-Dossary, S., Marfurt, K.J., 2006. 3D volumetric multispectral estimates of reflector curvature and rotation. Geophysics 71 (5), P41–P51. https://doi.org/10.1190/1.2242449.

Bahorich, M., Farmer, S., 1995. 3-D seismic discontinuity for faults and stratigraphic features: The coherence cube. Lead. Edge 14 (10), 1053–1058. https://doi.org/10.1190/1.1887523.

Bakulin, A., Grechka, V., Tsvankin, I., 2000. Estimation of fracture parameters from reflection seismic data—Part I: HTI model due to a single fracture set. Geophysics 65 (6), 1788–1802. https://doi.org/10.1190/1.1444863.

Barley, B., Summers, T., 2007. Multi-azimuth and wide-azimuth seismic: shallow to deep water, exploration to production. Lead. Edge 26 (4), 450–458. https://doi.org/10.1190/1.2723209.

Chen, F., Zong, Z., 2022. PP-wave reflection coefficient in stress-induced anisotropic media and amplitude variation with incident angle and azimuth inversion. Geophysics 87 (6), C155–C172. https://doi.org/10.1190/geo2021-0706.1.

Chen, H., Chen, T., Innanen, K.A., 2020. Estimating tilted fracture weaknesses from azimuthal differences in seismic amplitude data. Geophysics 85 (3), R135–R146. https://doi.org/10.1190/geo2019-0344.1.

Chen, F., Zong, Z., Yin, X., et al., 2023. Pressure and frequency dependence of elastic moduli of fluid-saturated dual-porosity rocks. Geophys. Prospect. 71 (8), 1599–1615. https://doi.org/10.1111/1365-2478.13395.

Cheng, Z., Bian, L., Chen, H., et al., 2022. Multiscale fracture prediction technique via deep learning, seismic gradient disorder, and aberrance: applied to tight sandstone reservoirs in the Hutubi block, southern Junggar Basin. Interpretation 10 (4), T647–T663. https://doi.org/10.1190/int-2021-0249.1.

Chopra, S., Marfurt, K., 2007. Curvature attribute applications to 3D surface seismic data. Lead. Edge 26 (4), 404–414. https://doi.org/10.1190/1.2723201.

Di, H., Gao, D., 2016. Improved estimates of seismic curvature and flexure based on 3D surface rotation in the presence of structure dip. Geophysics 81 (2), IM13–IM23. https://doi.org/10.1190/geo2015-0258.1.

Gersztenkorn, A., Marfurt, K.J., 1999. Eigenstructure-based coherence computations as an aid to 3-D structural and stratigraphic mapping. Geophysics 64 (5), 1468–1479. https://doi.org/10.1190/1.1444651.

Li, T., Wang, Z., Ma, S., et al., 2015. Summary of seismic attributes fusion method. Prog. Geophys. 30 (1), 378–385. https://doi.org/10.6038/pg20150155.

Li, F., Lyu, B., Qi, J., et al., 2021a. Seismic coherence for discontinuity interpretation. Surv. Geophys. 42, 1229–1280. https://doi.org/10.1007/s10712-021-09670-4.

Li, K., Zong, J., Fei, Y., et al., 2021b. Simultaneous seismic deep attribute extraction and attribute fusion. IEEE Trans. Geosci. Rem. Sens. 60, 1–10. https://doi.org/10.1109/TGRS.2021.3113075.

Liu, M., Jervis, M., Li, W., et al., 2020. Seismic facies classification using supervised convolutional neural networks and semisupervised generative adversarial networks. Geophysics 85 (4), O47–O58. https://doi.org/10.1190/geo2019-0627.1.

Ma, Z., Yin, X., Li, K., et al., 2022. Fourier coefficients variation with angle for fracture detection and fluid discrimination in tilted transversely isotropic media. Surv. Geophys. 43 (3), 775–813. https://doi.org/10.1007/s10712-022-09704-5.

Manning, T., Shane, N., Page, C., et al., 2007. Quantifying and increasing the value of multi-azimuth seismic. Lead. Edge 26 (4), 510–520. https://doi.org/10.1190/1.2723215.

Pan, X., Zhang, G., Yin, X., 2018. Azimuthal seismic amplitude variation with offset and azimuth inversion in weakly anisotropic media with orthorhombic symmetry. Surv. Geophys. 39, 99–123. https://doi.org/10.1007/s10712-017-9434-2.

Pan, X., Zhang, G., Yin, X., 2019. Amplitude variation with offset and azimuth inversion for fluid indicator and fracture weaknesses in an oil-bearing fractured reservoir. Geophysics 84 (3), N41–N53. https://doi.org/10.1190/geo2018-0554.1.

Qi, J., Li, F., Marfurt, K., 2017. Multiazimuth coherence. Geophysics 82 (6), O83–O89. https://doi.org/10.1190/geo2017-0196.1.

Roberts, A., 2001. Curvature attributes and their application to 3D interpreted horizons. First Break 19 (2), 85–100. https://doi.org/10.1046/j.0263-5046.2001.00142.x.

Shi, P., Yuan, S., Wang, T., et al., 2018. Fracture identification in a tight sandstone reservoir: a seismic anisotropy and automatic multisensitive attribute fusion framework. IEEE Geosci. Remote. S. 15 (10), 1525–1529. https://doi.org/10.1109/LGRS.2018.2853631.

Song, L., Yin, X., Zong, Z., et al., 2022. Semi-supervised learning seismic inversion based on spatio-temporal sequence residual modeling neural network. J. Pet. Sci. Eng. 208, 109549. https://doi.org/10.1016/j.petrol.2021.109549.

Song, L., Yin, X., Zhang, R., et al., 2024. Multi-azimuth seismic coherence fusion based on the azimuth focus detection. IEEE Geosci. Remote. S. https://doi.org/10.1109/LGRS.2024.3412092.

Sun, Q., Zong, Z., 2023. AVO inversion for low-frequency component of the model parameters based on dual-channel convolutional network. IEEE Trans. Geosci. Rem. Sens. 61, 1–14. https://doi.org/10.1109/TGRS.2023.3333341.

Sun, Q., Zong, Z., Li, X., 2024. Probabilistic seismic inversion based on physics-guided deep mixture density network. Pet. Sci. 21 (3), 1611–1631. https://doi.org/10.1016/j.petsci.2023.12.015.

Wang, K., Yin, X., Ma, Z., et al., 2023. Fault prediction method based on multi-azimuth coherence attribute. Chin. J. Geophys. 66 (9), 3828–3839. https://doi.org/10.6038/cjg2022Q0294.

Xiang, W., Yin, X., Ma, Z., et al., 2022. Fracture detection with azimuthal seismic amplitude difference inversion in weakly monoclinic medium. IEEE Trans. Geosci. Rem. Sens. 60, 1–16. https://doi.org/10.1109/TGRS.2022.3224990.

Xiong, W., Ji, X., Ma, Y., et al., 2018. Seismic fault detection with convolutional neural network. Geophysics 83 (5), O97–O103. https://doi.org/10.1190/geo2017-0666.1.

Yan, B., Wang, T., Ji, Y., et al., 2022. Multidirectional coherence attribute for discontinuity characterization in seismic images. IEEE Geosci. Remote. S. 19, 1–5. https://doi.org/10.1109/LGRS.2022.3151686.

Zhou, S., Zhong, H., 2024. Seismic attribute fusion technology based on SSAE. Prog. Geophys. 39 (2), 647–660. https://doi.org/10.6038/pg2024HH0215.